

Excited States of Ladder-type Poly-p-phenylene Oligomers

Jörg Rissler and Heinz Bässler

*Institut für Physikalische Chemie, Kern-Chemie und Makromolekulare Chemie, Philipps
Universität Marburg, Hans-Meerwein-Straße, D-35032 Marburg, Germany*

Florian Gebhard

Fachbereich Physik, Philipps Universität Marburg, D-35032 Marburg, Germany

Peter Schwerdtfeger

*The University of Auckland, Department of Chemistry, Private Bag 92019, Auckland, New
Zealand*

(Preprint version of November 23, 2000)

Abstract

Ground state properties and excited states of ladder-type paraphenylene oligomers are calculated applying semiempirical methods for up to eleven phenylene rings. The results are in qualitative agreement with experimental data. A new scheme to interpret the excited states is developed which reveals the excitonic nature of the excited states. The electron-hole pair of the S_1 -state has a mean distance of approximately 4 Å.

I. INTRODUCTION

The investigation of π -conjugated polymers is in many ways affected by the structural disorder in these systems. In contrast, the ladder-type poly-p-phenylenes (LPPP) [1] offer the opportunity to study large, rod-like chains of planarised phenylene units. As a consequence, the π -system might spread out over an entire polymer and a vibronic resolution of the $S_1 \leftarrow S_0$ transition is discernible [2]. In order to deduce some characteristics of the polymeric films [3], like the effective conjugation length, several oligomers have been synthesized in the past to study the low-lying electronic excited states of the polymer [4,5].

Photoconduction in LPPP films [6] has been measured as a function of the energy of the exciting light, too. A typical small plateau of the photocurrent occurs between the absorption edge and its steep rise at higher energies and extends in this case over 1.6 eV. This behavior of the photocurrent which does not follow directly the absorption features is sometimes called “abatic”.

One possible explanation for this effect rests on the interpretation of the electronic excited states for the individual molecules. Excited states of π -conjugated molecules are usually described as Coulomb bound electron-hole pairs. This physical picture originates from solid-state physics of (organic) semi-conductors. Therefore, these molecular states are often referred to as excitons, although they have to be clearly distinguished from the extended band states in a crystal.

A reasonable estimate of the exciton binding energy in conjugated polymers has been determined, e.g., by scanning tunneling spectroscopy measurements [7] which have lead to a value of about 3.5 eV. Excited states with a smaller value, and larger electron-hole distance, respectively, should be more susceptible to the separation via an external electric field. Following this idea, the conjecture has been brought forward that such a state is responsible for the steep rise of the photocurrent in poly-phenylene-vinylene (PPV) [8]. Later on, another explanation has followed based on the excess photon energy which is converted to the vibrational heat bath [9]. The latter proposal is now widely accepted.

In order to test these concepts for excited states of π -conjugated systems, several oligomers of the LPPP type with up to eleven phenylene rings are investigated in this work. The study of oligomers instead of an (infinite) polymer follows the above mentioned approach and allows the direct comparison with experiment. The main difference to the experiments in condensed phases is the restriction to single chains in the vacuum.

As the experimentally used molecules are computationally too demanding one has to replace the large aliphatic substituents attached to LPPP by hydrogen (see Figure 1 and Table I). This should have only negligible effects on the optical properties, which are governed by the frontier orbitals of π -symmetry. These aliphatic substituents are only necessary for the better solubility of the polymer, or to prohibit the formation of aggregates in the film (R_3 = methyl in Figure 1).

Since the systems studied here reach the size of the effective conjugation length proposed for LPPP (about 14 phenylene rings [4,2]), ab-initio or density functional methods are not applicable, and one has to assent to less expensive semiempirical methods (AM1, INDO/S; see below). Thus, the wave functions of the corresponding ground states are the INDO (intermediate neglect of differential overlap) Slater determinants $|\Phi_0^{\text{INDO}}\rangle$ [10]. For the excited states $|\Phi_s^{\text{CIS}}\rangle$ (see equation 16), the INDO/S expansion is used in the spin-singlet sector. The

excited states with dominant oscillator strengths will be addressed as S_1 for the first excited state, S_m for the intermediate excited state and S_F for the high energy, “Frenkel-type” state. The electronic ground state will be denoted as $S_0 \equiv |\Phi_0^{\text{INDO}}\rangle$.

The article is organized as follows. In Sect. II, the semiempirical approach is briefly described. In Sect. III, the results for the geometric structure of the oligomers and their spectra are presented. The main part of this article, Sect. IV, focuses on the development of a general interpretation scheme for excited-state wave functions. Its application to INDO/S wave functions leads in a straightforward way to the interpretation of the excited states as bound electron-hole pairs. A short conclusion closes the presentation.

II. METHODS

Although it is not feasible to calculate the higher oligomers by first-principle methods, the oligomer with two phenylene rings ($n = 0.5$) has been calculated at MP2/6-31G* level [11,12](Møller-Plesset Perturbation Theory of second order). The results are used as a reference for the semiempirical methods.

Following a procedure of Brédas *et al.* [13], one has to choose a semiempirical method which yields reliable geometric structures. In the present case the Austin semiempirical parametrization (AM1) [14] gives an almost exact agreement with the MP2 results (cf. $\sum |\Delta r_{C-C}|$ for the bond lengths in Table II). This method will therefore be used to calculate the geometric structure of the ground states. Note, however, that the PM3 method [15] yields better results for zero-point vibrational energies (ZPE).

The AM1 and MP2 calculations have been carried out on a IBM/SP2 computer using the GAUSSIAN94 (Rev. D4) [16] program package. All minima are characterized by diagonalization of the Hessian Matrix, whereby the zero-point energies (ZPE) have been obtained, too. The latter will be given unscaled throughout the paper.

In the next step, excited singlet states are calculated using Zerner’s INDO/S method [17] based on the minimum AM1 structures from the electronic ground states. Thus it is clear that geometric relaxation effects in the excited state are neglected. The active CI space consists of the 22 highest occupied and the 22 lowest unoccupied molecular orbitals. This is the biggest active space possible within the used program package and it contains orbitals of σ symmetry for some oligomers as well. As expected, the dominant configuration state functions in the wave function describe π - π^* excitations. The calculation of the spectra have been accomplished on a PentiumIII-PC using the program package CAChe 3.1 [18].

In order to get a more realistic view of the calculated line spectra, Gaussian peaks are least-square fitted to the INDO/S oscillator strengths. This procedure masks transitions with moderate oscillator strengths which are close in energy to a dominant transition. This is especially the case for the high-energy region of the spectrum, in which strong $S_F \leftarrow S_0$ transitions cover others. The hidden states are not visible in the optical spectrum, and consist of a number of important configurations sensitive to the size of the active CI space (Figure 3). The remaining part of the spectra comprises only features with one transition, except in two cases, where two almost identical states are close together. In these cases only one state will be discussed (the $S_1 \leftarrow S_0$ transition for the $n = 0.5$ oligomer and the $S_m \leftarrow S_0$ transition for the trimer; see discussion below).

III. RESULTS FOR GEOMETRY AND OPTICAL SPECTRA

A. Geometry

All structures have been optimized without any symmetry constraints. Therefore, the geometries only fit to certain point groups within crystallographic accuracy ($\pm 0.001 \text{ \AA}$, $\pm 2^\circ$). The resulting point groups are equivalent to ones suggested by the simple Lewis-type structure, see Figure 1. Oligomers with an even number of phenylene rings adopt C_{2v} symmetry. Those with an odd number adopt C_{2h} symmetry. The C–C bond lengths range between about 1.380 \AA and about 1.500 \AA . Figure 2 shows the MP2 result for the $n = 0.5$ oligomer as an example.

As the smallest C–C bond distance in a methylene bridge is 1.503 \AA long, they are assigned to single bonds. As a consequence, the hydrogen atoms of the methylene bridge do not participate in the conjugated system, although this would be allowed. This supports the validity of neglecting the aliphatic substituents.

B. Optical spectra

In Figure 3 the (vibronically unresolved) calculated spectra of LPPP oligomers are plotted. A comparison with measured fluorescence spectra of different oligomers [5] shows qualitative agreement, i.e., they show a broad $S_1 \leftarrow S_0$ transition which is shifting to lower energies with increasing system size. As one would expect for the S_1 state, the HOMO–LUMO excitation is the dominant one. HOMO (LUMO) refers to the highest occupied (lowest unoccupied) molecular orbital in the INDO ground state.

A second interesting feature can be seen in the calculations for the oligomers with five and more rings. It will be referred to as the $S_m \leftarrow S_0$ transition, because it is energetically in the middle between the S_1 state and the high energy region. In the S_m state the dominant determinants are built by the substitution of the HOMO by the LUMO+2 and the substitution of the HOMO–1 by the LUMO+1. The position of the $S_m \leftarrow S_0$ transition also shifts to lower energies with increasing oligomer length. This is not discernible in the experimental spectra because of the small corresponding oscillator strengths.

Finally, both sets of spectra show a steep rise at around 5.40 eV which is dominated by a transition at approximately 5.85 eV for every oligomer. This transition will be called the $S_F \leftarrow S_0$ transition, as the S_F state shows a high degree of localization (i.e., a “Frenkel” state), which will become clear later in the discussion. The S_F state is determined by several configuration state functions, where low-lying occupied molecular orbitals are exchanged by orbitals with high energy.

In Figure 4 the energy of all three optically important transitions is drawn as a function of the reciprocal number of phenylene rings in the molecule. The transitions of the S_1 and the S_m states show a strong linear dependence, whereas the energy of the $S_F \leftarrow S_0$ transitions hardly changes with system size, in agreement with the experimental observation. Despite this qualitative agreement, a quantitative comparison with the experimental values for the effective conjugation length [4] is not possible, since the theoretical curve leads to an unphysical negative value. The main reason for this error is the neglect of the polarization energy in the calculations which stabilizes the excited states in the condensed phases in the

experiments. Moreover, the linear extrapolations for the transitions to the S_m and the S_1 states suggest a crossing of the two energies which must not be taken for granted at this stage.

From the electronic dipole transition moments \mathbf{M} for the $S_1 \leftarrow S_0$ transitions, one obtains an estimate for the radiative fluorescence lifetimes τ for every oligomer, using

$$\mathbf{M} = e \left\langle \Phi_s^{\text{CIS}} \left| \sum_i z_i \vec{r}_i \right| \Phi_0^{\text{INDO}} \right\rangle, \quad (1a)$$

$$\tau = \frac{3\hbar c^3}{8\pi\omega^3 |\mathbf{M}|^2}. \quad (1b)$$

Here, e is the elementary charge, \vec{r}_i is the position vector of the i -th particle of charge $z_i e$, \hbar is Planck's constant, c is the speed of light, and $\hbar\omega$ is the energy of the transition, all quantities measured in cgs units. The lifetimes τ show a linear dependence on the reciprocal number of phenylene rings, see Figure 5. Here, the value of several hundred picoseconds for the large oligomers is in quantitative agreement with the experimental value of about 300 ps for the polymer, measured in an organic matrix [19]. Under the assumption of a linear relation between τ and the inverse of the oligomer length, one finds from the data in Table IV that a value of $\tau_{\text{polymer}} = 300$ ps corresponds to an effective conjugation length of about 20 phenylene rings, in reasonable agreement with the value of 14 rings estimated from other optical experiments [4,2].

IV. INTERPRETATION

A. General considerations

For an interpretation the wave functions for the ground state and the excited states need to be related to experimentally observable quantities. The optical absorption at frequency ω is proportional to the real part of the optical conductivity, as given by the Kubo formula [20]

$$\text{Re} [\sigma(\omega > 0)] = \frac{\text{Im} [\chi_{jj}(\omega > 0)]}{\omega}, \quad (2)$$

where $\chi_{jj}(\omega)$ is the current-current correlation function,

$$\begin{aligned} \chi_{jj}(\omega > 0) &= - \left\langle \Phi_0 \left| \hat{j} \frac{1}{E_0 - \hat{H} + \omega + i\eta} \hat{j} \right| \Phi_0 \right\rangle \\ &= - \sum_{|\Phi_s\rangle} \frac{|\langle \Phi_s | \hat{j} | \Phi_0 \rangle|^2}{\omega - (E_s - E_0) + i\eta}. \end{aligned} \quad (3)$$

Here, \hat{H} is the Hamilton operator of the system, $|\Phi_s\rangle$ are its eigenstates with energies E_s ($s = 0, 1, 2, \dots$), $\hbar \equiv 1$, and $\eta = 0^+$ is positive infinitesimal. Therefore, the real part of the optical conductivity may be written as

$$\text{Re} [\sigma(\omega > 0)] = \frac{\pi}{\omega} \sum_{|\Phi_s\rangle} |\langle \Phi_s | \hat{j} | \Phi_0 \rangle|^2 \delta(\omega - (E_s - E_0)). \quad (4)$$

The current operator is defined by

$$\hat{j} = \sum_{\sigma} \sum_{m,n} p_{m,n} \hat{C}_{n,\sigma}^{\dagger} \hat{C}_{m,\sigma} , \quad (5)$$

where $\hat{C}_{n,\sigma}^{\dagger}$, $\hat{C}_{n,\sigma}$ are creation and annihilation operators for electrons with spin $\sigma = \uparrow, \downarrow$ in the molecular orbitals ϕ_n , and $p_{m,n}$ is the matrix element between the corresponding one-particle states.

Equation (4) is readily interpreted. The absorption of a photon with energy ω induces an excitation between the ground state $|\Phi_0\rangle$ and the excited states $|\Phi_s\rangle$ with energy $\omega = E_s - E_0$. The amplitude for this absorption process

$$A_{0,s} = \langle \Phi_s | \hat{j} | \Phi_0 \rangle \quad (6)$$

determines the oscillator strength, $f_{0,s} \propto |A_{0,s}|^2$.

For a further analysis of the amplitudes $A_{0,s}$, the current operator is expressed in terms of the field operators,

$$\hat{\Psi}_{\sigma}^{\dagger}(\vec{x}) = \sum_n \phi_n^*(\vec{x}) \hat{C}_{n,\sigma}^{\dagger} , \quad (7a)$$

$$\hat{\Psi}_{\sigma}(\vec{x}) = \sum_n \phi_n(\vec{x}) \hat{C}_{n,\sigma} , \quad (7b)$$

which create/annihilate an electron with spin σ at \vec{x} . From the completeness of the molecular orbitals $\phi_n(\vec{x})$ one readily obtains

$$\hat{j} = \sum_{\sigma} \int d\vec{x} d\vec{y} j(\vec{x}, \vec{y}) \hat{\Psi}_{\sigma}^{\dagger}(\vec{x}) \hat{\Psi}_{\sigma}(\vec{y}) \quad (8)$$

with

$$j(\vec{x}, \vec{y}) = \sum_{n,m} p_{m,n} \phi_n(\vec{x}) \phi_m^*(\vec{y}) . \quad (9)$$

Therefore, the amplitudes can be cast into the form

$$A_{0,s} = \sum_{\sigma} \int d\vec{x}_e d\vec{x}_h j(\vec{x}_e, \vec{x}_h) A_{0,s}^{\sigma}(\vec{x}_e, \vec{x}_h) , \quad (10)$$

where the particle-hole amplitudes

$$A_{0,s}^{\sigma}(\vec{x}_e, \vec{x}_h) = \langle \Phi_s | \hat{\Psi}_{\sigma}^{\dagger}(\vec{x}_e) \hat{\Psi}_{\sigma}(\vec{x}_h) | \Phi_0 \rangle \quad (11)$$

are given by the overlap between the excited state $|\Phi_s\rangle$ and the ground state $|\Phi_0\rangle$ with an electron at \vec{x}_e and a hole at \vec{x}_h (if $\vec{x}_e \neq \vec{x}_h$).

It is thus seen that the quantities $A_{0,s}^{\sigma}(\vec{x}_e, \vec{x}_h)$ allow to address the question in how far a given excited state $|\Phi_s\rangle$ may be viewed as an electron-hole excitation of the ground state, and they directly enter the Kubo formula for the optical conductivity. Note that the analysis of (11) does not require the full spatial dependence of the many-particle wave functions $|\Phi_s\rangle$ or $|\Phi_0\rangle$ as in [8,21] or the density-density correlation function of the ground state as in [22].

The matrix elements for the current operator, $j(\vec{x}_e, \vec{x}_h)$ in (9), do not change much over atomic distances. Therefore, it is usually sufficient to introduce the coarse-grained densities for the electron-hole content of $|\Phi_s\rangle$ with respect to $|\Phi_0\rangle$,

$$P_{0,s}(i, j) = \sum_{\sigma} \int d\vec{x}_e d\vec{x}_h \left| A_{0,s}^{\sigma}(\vec{x}_e, \vec{x}_h) \right|^2 \Theta(\vec{x}_h - \vec{r}_i) \Theta(\vec{x}_e - \vec{r}_j) , \quad (12)$$

where

$$\Theta(\vec{x} - \vec{r}_i) = \begin{cases} 1 & , \text{ if } \vec{x} - \vec{r}_i \in V_i \\ 0 & , \text{ else} \end{cases} \quad (13)$$

is the step function for the (atomic) volume V_i around atom i . $P_{0,s}(i, j)$ is the overlap density between the excited $|\Phi_s\rangle$ and the ground state $|\Phi_0\rangle$ with an electron-hole pair around the nuclei at i and j , respectively.

Equation (11) is exact and applies to all quantum-mechanical systems. It is currently under investigation for the numerical analysis of quantum lattice systems with the density matrix renormalisation group (DMRG) method [23]. In the next subsection, the present case of INDO/S wave functions will be studied in more detail.

B. Application to INDO/S

As described earlier, the ground state is approximated as an INDO Slater determinant

$$|\Phi_0\rangle \approx |\Phi_0^{\text{INDO}}\rangle = \prod_{\sigma} |\Phi_{\sigma,0}^{\text{INDO}}\rangle = \prod_{\sigma} \prod_{1 \leq a \leq n} \hat{C}_{a,\sigma}^{\dagger} |\text{vacuum}\rangle , \quad (14a)$$

$$|\Phi_{\sigma,0}^{\text{INDO}}\rangle = \frac{1}{n!} \int d\vec{x}_1 \dots d\vec{x}_n \text{Det} [\phi_a(\vec{x}_i)] \Psi_{\sigma}^{\dagger}(\vec{x}_1) \dots \Psi_{\sigma}^{\dagger}(\vec{x}_n) |\text{vacuum}\rangle , \quad (14b)$$

where the molecular orbitals $\phi_a(\vec{x}_i)$ ($1 \leq a \leq n$) are expressed as a linear combination of spatial atomic orbitals (AOs) $\chi_b(\vec{x})$

$$\phi_a(\vec{x}_i) = \sum_b^{\text{AOs}} d^a(b) \chi_b(\vec{x}_i) . \quad (15)$$

The atomic orbitals are centered at certain nuclei such that $b \equiv (\vec{r}_b, \beta_b)$ comprises the orbital type ($\beta_b = s, p, d \dots$) and its position \vec{r}_b .

The spin singlet excited-state wave functions are described as linear combinations of singly-excited configuration state functions

$$|\Phi_s\rangle \approx |\Phi_s^{\text{CIS}}\rangle , \quad (16a)$$

$$|\Phi_s^{\text{CIS}}\rangle = \sqrt{\frac{1}{2}} \sum_{\sigma} \sum_{a,r} c_{a,r} \hat{C}_{r,\sigma}^{\dagger} \hat{C}_{a,\sigma} |\Phi_0^{\text{INDO}}\rangle , \quad (16b)$$

where the indices a and r refer to the active space of occupied and virtual molecular orbitals, respectively.

With these approximations for $|\Phi_0\rangle$ and $|\Phi_s\rangle$, it is obvious that the coordinates of the added electron enter (11) only through the virtual MOs ϕ_r whereas the hole is described by the eliminated, occupied MOs ϕ_a ,

$$\begin{aligned} A_{0,s}^\sigma(\vec{x}_e, \vec{x}_h) &\approx \langle \Phi_s^{\text{CIS}} | \hat{\Psi}_\sigma^\dagger(\vec{x}_e) \hat{\Psi}_\sigma(\vec{x}_h) | \Phi_0^{\text{INDO}} \rangle \\ &= \sqrt{\frac{1}{2}} \sum_{a,r} c_{a,r}^* \phi_r^*(\vec{x}_e) \phi_a(\vec{x}_h) . \end{aligned} \quad (17)$$

To make further progress, one has to address the coarse-grained densities $P_{0,s}(i, j)$ in (12),

$$\begin{aligned} P_{0,s}(i, j) &\approx P_{0,s}^{\text{INDO/S}}(i, j) \\ P_{0,s}^{\text{INDO/S}}(i, j) &= \int d\vec{x}_e d\vec{x}_h \left| \sum_{a,r} c_{a,r}^* \phi_r^*(\vec{x}_e) \phi_a(\vec{x}_h) \right|^2 \Theta(\vec{x}_h - \vec{r}_i) \Theta(\vec{x}_e - \vec{r}_j) \\ &= \sum_{\beta_i, \beta_j} \sum_{\substack{a, r \\ a', r'}} c_{a,r}^* c_{a',r'} (d^r(\vec{r}_j, \beta_j))^* d^{r'}(\vec{r}_j, \beta_j) (d^{a'}(\vec{r}_i, \beta_i))^* d^a(\vec{r}_i, \beta_i) . \end{aligned} \quad (18)$$

In the last step the INDO approximation [10] and the orthogonality of the atomic orbitals on the same atom were used, i.e.,

$$\int d\vec{x} \Theta(\vec{x} - \vec{r}_j) \chi_b^*(\vec{x}) \chi_{b'}(\vec{x}) \approx \delta_{b,b'} \delta_{\vec{r}_b, \vec{r}_j} . \quad (19)$$

Recall that $d^r(\vec{r}_j, \beta_j)$ denote AO coefficients, and $c_{a,r}$ are the CI coefficients of the CIS wave function. In this case, one may verify that $\sum_{i,j} P_{s,0}(i, j) = 1$, if one takes into account the INDO approximation and the normalization of $|\Phi_s^{\text{CIS}}\rangle$ in (16),

$$1 = \langle \Phi_s^{\text{CIS}} | \Phi_s^{\text{CIS}} \rangle = \int \left| \sum_{a,r} c_{a,r}^* \phi_r^*(\vec{x}_e) \phi_a(\vec{x}_h) \right|^2 d\vec{x}_e d\vec{x}_h = \sum_{i,j}^{\text{nuclei}} P_{s,0}^{\text{INDO/S}}(i, j) . \quad (20)$$

Therefore, $P_{s,0}^{\text{INDO/S}}(i, j)$ may be viewed as a discrete probability function for finding a hole around the nucleus i and an electron around the nucleus j . This simplification is only valid in the INDO/S approximation.

A check can be made, whether the values of $P_{s,0}^{\text{INDO/S}}(i, j)$ carry significant weight corresponding to AOs of σ symmetry. It turns out that this weight is vanishingly small, and one can sum all contributions of the AOs of an atom without losing information.

One has to verify that the detected electron-hole correlations for an excited state really stem from the electron-hole interaction rather than from a coincidence of the motion of two independent particles confined to a small molecule. Therefore, the quantity

$$A_{0,\text{H}\rightarrow\text{L}}^\sigma = \langle \Phi_{\text{H}\rightarrow\text{L}} | \hat{\Psi}_\sigma^\dagger(\vec{x}_e) \hat{\Psi}_\sigma(\vec{x}_h) | \Phi_0^{\text{INDO}} \rangle \quad (21)$$

has been investigated according to the scheme (11). Here, $|\Phi_{\text{H}\rightarrow\text{L}}\rangle$ is the INDO wave function where the HOMO is substituted by the LUMO. This corresponds to the pure “band-like” excitation, i.e., in a CIS state representation this configuration state function has the coefficient $c_{a,r} = 1$ for $a = \text{HOMO}$, $r = \text{LUMO}$, and all other coefficients are set to zero.

Given the $P_{s,0}^{\text{INDO/S}}(i,j)$ an expectation value $\langle E \rangle$ of the distance of the electron-hole pair can be calculated with the help of the bond lengths $r(i,j) = |\vec{r}_i - \vec{r}_j|$ of the molecule,

$$\langle E \rangle_{s,0} = \sum_{i,j} P_{s,0}^{\text{INDO/S}}(i,j) r(i,j) . \quad (22)$$

The standard deviation $\sigma_{s,0}$ is equally accessible,

$$(\sigma_{s,0})^2 = \sum_{i,j} (r(i,j) - \langle E \rangle_{s,0})^2 P_{s,0}^{\text{INDO/S}}(i,j) . \quad (23)$$

In small molecules, the confinement of the oligomers will determine the distance of the electron-hole pair. In larger molecules, if the interaction between hole and electron is weak, $\langle E \rangle_{s,0}$ and $\sigma_{s,0}$ will increase with system size since the particles move essentially independently through the molecule. On the other hand, the interaction between electron and hole may keep them together at a fixed distance even though the size of the molecule increases. Such a bound electron-hole pair may lead to a constant value of $\langle E \rangle_{s,0}$ and $\sigma_{s,0}$ for every system size. Note, however, $\langle E \rangle_{s,0}$ and $\sigma_{s,0}$ only contain an information about the overall extension of an excitation but may fail to describe the localization of an electron-hole pair onto segments of the molecule; an example of this situation is given below.

In order to get a more pictorial way of the electron-hole pair distribution, one may concentrate on a quasi one-dimensional chain of carbon atoms; Figure 6 shows how those chains are chosen. When $P_{s,0}(i,j)$ is plotted for this chain a bound electron-hole pair will show large values along the diagonal of the plot and vanishingly small values in the off-diagonal regions. Unbound pairs will lead to the opposite situation.

The two-dimensional distribution $P_{s,0}(i,j)$ can be further smoothed into

$$\overline{P}_{s,0}(r) = \int_{r-\Delta r/2}^{r+\Delta r/2} dr' \sum_{i,j}^{\text{nuclei}} P_{s,0}(i,j) \delta(r' - |\vec{r}_i - \vec{r}_j|) , \quad (24)$$

which is solely a function of the electron-hole distance. The choice of $\Delta r = 1.8 \text{ \AA}$ gives smooth curves as a function of r . $\overline{P}_{s,0}(r)$ gives the most concise description of the electron-hole excitation.

C. Results

The $P_{s,0}^{\text{INDO/S}}(i,j)$ matrix has been calculated for the states, whose transitions are of significant oscillator strength in the spectra: The S_1 , the S_m , and the S_F state.

First, the state S_1 is discussed. As seen from Figure 7, no bound state is formed for only two phenylene rings. In fact, the molecular confinement is dominant up to a chain length of four phenylene rings. For five phenylene rings, see Figure 8, and larger systems, a bound electron-hole pair is discernible. The shape of $P_{S_1,0}(i,j)$ in the plot along the one-dimensional chain does not change for systems larger then five phenylene rings. The S_1 state clearly corresponds to a strongly bound electron-hole pair.

Figure 9 shows the average electron-hole separation and the corresponding standard deviation for the S_1 state as a function of system size. They saturate for more than five

phenylene rings, $\langle E \rangle_{S_{1,0}} \approx 4 \text{ \AA}$. This is in reasonable agreement with the experimental value of 7 \AA obtained from electro-absorption measurements [2]. Some results of electron energy-loss spectroscopy, however, seem to hint at a totally different behavior of the excited states: they are supposed always to increase with increasing length of the oligomer [24]. At present, the reason for this discrepancy is not clear.

The saturation behavior for $\langle E \rangle_{S_{1,0}}$ and the apparently large saturation value for the standard deviation $\sigma_{S_{1,0}} \approx 3 \text{ \AA}$ are readily understood from the “smoothed” probability distribution $\bar{P}_{S_{1,0}}(r)$, see (24). As seen in Figure 10, $\bar{P}_{S_{1,0}}(r \rightarrow 0)$ decreases with increasing system size, the whole distribution broadens, and develops a maximum around $r_m = 4 \text{ \AA}$. For oligomers with five and more phenylene rings the distribution does not change significantly. Since at the same time the system grows, the values of $\langle E \rangle_{S_{1,0}}$ and $\sigma_{S_{1,0}}$ saturate. The relatively large values of $\sigma_{S_{1,0}}$ are due to the location of the maximum of the distribution at a finite value of r_m . Finally, Figure 11 shows the probability distribution $P_{S_{1,0}}^{\text{INDO/S}}(i, j)$ for the largest oligomer with eleven phenylene rings ($n = 5$).

Next, the state S_m is addressed. Brédas and coworkers have located a state in the calculated spectrum of poly-p-phenylene-vinylene (PPV), which they assign to a charge transfer state. In this context this state is equivalent to an unbound electron-hole pair. The optical transition to this charge transfer state is in the same region as the steep increase of the photocurrent in the respective polymeric film. As a result, they conclude that the population of this state is responsible for this “abatic” behavior of the photocurrent. The S_m state obtained in the present calculation lies in the same region as the charge-transfer state in PPV, that is between the S_1 and the high-energy states. The question is, whether the S_m state is a charge transfer state or not.

As seen in Figure 12, the S_m state shows almost constant values of $\langle E \rangle_{S_m,0}$ and $\sigma_{S_m,0}$. A rise in these values occurs for the $n = 5$ oligomer which hints at unbound states for larger systems. This idea, however, is not supported by a more detailed look at the graphs for $\bar{P}_{S_m,0}(r)$ as a function of oligomer length, see Figure 13, and the results for $P_{S_m,0}(i, j)$ for the largest oligomer, see Figure 14. The curves are qualitatively the same as for the corresponding S_1 states. For example, compare Figures 11 and 14: $P_{S_{1,0}}(i, j)$ and $P_{S_m,0}(i, j)$ are essentially zero in the off-diagonal regions. Similarly, the curves $\bar{P}_{S_m,0}(r)$ as a function of oligomer length resemble those of $\bar{P}_{S_{1,0}}(r)$, compare Figures 10 and 13. The only difference to the S_1 state is the localization of the excitation to three parts of the molecule in S_m . Because of this, one cannot interpret this state as an unbound electron-hole pair or exciton, and consequently no explanation for the rise of the photocurrent of LPPP at about 4.0 eV can be given at this level of theory. This is in line with the assumption that local heating due to excess energy is the reason for the behavior of the photocurrent [9] and not the nature of the optically accessible states.

Lastly, for the S_F state, the mean electron-hole separation does not saturate but grows with system size, see Fig. 15. From such an analysis one might conclude a delocalized state. On the contrary, for the S_F state the degree of localization is *higher* than in the other two excited states, and the electron-hole pair is actually restricted to every single phenylene ring. As can be seen from Figures 16 and 17, the apparent lack of convergence in $\langle E \rangle_{S_F,0}$ and $\sigma_{S_F,0}$ relates to the fact that isolated electron-hole pairs on chain segments can be linearly superimposed, i.e., an extended state can be formed which, nevertheless, does not contribute to the conductivity. As for the states S_1 and S_m , there is no spreading of $P_{S_F,0}(i, j)$ into

off-diagonal regions with increasing system size, and the smoothed distribution function $\overline{P}_{S_F,0}(r)$ displays the same trends as before.

So far, every state investigated can be regarded as a bound electron-hole pair with different degrees of localization. They are molecular analogues of the excitons in the physics of semiconductors. In order to see the differences to a pure “band excitation”, the analysis is repeated for $|\Phi_{H \rightarrow L}\rangle$, see (21). As expected, and confirmed in Figures 18, 19, and 20, the motion of electron and hole in the molecule is uncorrelated. In contrast to the excitonic cases before, the almost linear increase of the mean electron-hole separation and its variance as a function of system size in Figure 18 is accompanied by a broadening and flattening of the smoothed distribution function $\overline{P}_{H \rightarrow L,0}(r)$, see Figure 19. As seen from Figure 20 there is considerable weight in the off-diagonal region in the probability distribution $P_{H \rightarrow L,0}(i, j)$, which actually looks like a half sphere. Hence, the excitonic behavior of the states S_1 , S_m , and S_F is genuine, and not just a coincidence in the uncorrelated motion of an electron and a hole in a restricted geometry.

V. CONCLUSION

The ground and singlet excited states of various oligomers of LPPP have been described with semiempirical methods. A qualitative agreement was achieved with the experimental absorption spectra, especially for the measurements of the fluorescence lifetime, and the mean electron-hole distance. A new analysis of the excited states has been given. As in optical absorption experiments, the overlap matrix elements between excited states and the ground state with an electron-hole pair are studied as a function of their respective positions on the oligomers. Excited states with high oscillator strengths are found to be bound electron-hole pairs. Therefore, no explanation of the abatic onset of the photocurrent in LPPP films can be given at this level of a microscopic theory.

ACKNOWLEDGMENTS

This work has been made possible with the kind technical support of Prof. Frenking, and the financial support of the Graduiertenkolleg “Optoelektronik mesoskopischer Halbleiter” as well as the AURC and the Marsden Fund in Wellington.

REFERENCES

- [1] U. Scherf, A. Bohnen and K. Müllen, *Macromol. Chem.* **193**, 1127 (1992).
- [2] M. G. Harrison, S. Möller, G. Weiser, G. Urbasch, R. F. Mahrt and H. Bässler, *Phys. Rev. B* **60**, 8650 (1999).
- [3] G. Wegner and K. Müllen, *Electronic Materials: The Oligomer Approach*, (Wiley/VCH, Weinheim, 1996).
- [4] J. Grimme, M. Kreyenschmidt, F. Uckert, K. Müllen, and U. Scherf, *Adv. Mater.* **7**, 292 (1995).
- [5] T. Pauck, H. Bässler, J. Grimme, U. Scherf and K. Müllen, *Chem. Phys.* **210**, 219 (1996).
- [6] S. Barth, H. Bässler, U. Scherf and K. Müllen, *Chem. Phys. Lett.* **288**, 147 (1998).
- [7] S. F. Alvarado, P. F. Seidler, D. G. Lidzey, and D. D. G. Bradley, *Phys. Rev. Lett.* **81**, 1082 (1998).
- [8] A. Köhler, D. A. dos Santos, D. Beljonne, Z. Shuai, J.-L. Brédas, A. B. Holmes, A. Kraus, K. Müllen, and R. H. Friend, *Nature* **392**, 903 (1998).
- [9] V. I. Archipov, E. V. Emelianova and H. Bässler, *Phys. Rev. Lett* **82**, 1321 (1999).
- [10] J. A. Pople, D. L. Beveridge and P. A. Dobosh, *J. Chem. Phys.* **47**, 2026 (1967).
- [11] C. Möller and M. S. Plesset, *Phys. Rev.* **46**, 618 (1934).
- [12] R. Ditchfield, W. J. Hehre and J. A. Pople, *J. Chem. Phys.* **54**, 724 (1971).
W. J. Hehre, R. Ditchfield and J. A. Pople, *J. Chem. Phys.* **56**, 2257 (1972).
P. C. Hariharan and J. A. Pople, *Mol. Phys.* **27**, 209 (1974).
M. S. Gordon, *Chem. Phys. Lett.* **76**, 163 (1980).
P. C. Hariharan and J. A. Pople, *Theo. Chim. Acta* **28**, 213 (1973).
G. A. Petersson, A. Bennett, T. G. Tensfeldt, M. A. Al-Laham, W. A. Shirley and J. Mantzaris, *J. Chem. Phys.* **89**, 2193 (1988).
- [13] J. Cornil, D. Beljonne, D. A. dos Santos, Z. Shuai and J.-L. Brédas, *Synth. Met.* **78**, 209 (1996).
- [14] J. S. Dewar, E. G. Zoebisch and E. F. Healy, *J. Am. Chem. Soc.* **107**, 3902 (1985).
- [15] J. J. P. Stewart, *J. Comp. Chem.* **10**, 221 (1989).
- [16] Gaussian 94, Revision D4; M.J. Frisch, G.W. Trucks, H.B. Schlegel, G.E. Scuseria, M.A. Robb, J.R. Cheeseman, V.G. Zakrzewski, J.A. Montgomery, Jr., R.E. Stratmann, J.C. Burant, S. Dapprich, J.M. Millam, A.D. Daniels, K.N. Kudin, M.C. Strain, O. Farkas, J. Tomasi, V. Barone, M. Cossi, R. Cammi, B. Mennucci, C. Pomelli, C. Adamo, S. Clifford, J. Ochterski, G.A. Petersson, P.Y. Ayala, Q. Cui, K. Morokuma, D.K. Malick, A.D. Rabuck, K. Raghavachari, J.B. Foresman, J. Cioslowski, J.V. Ortiz, A.G. Baboul, B.B. Stefanov, G. Liu, A. Liashenko, P. Piskorz, I. Komaromi, R. Gomperts, R.L. Martin, D.J. Fox, T. Keith, M.A. Al-Laham, C.Y. Peng, A. Nanayakkara, C. Gonzalez, M. Challacombe, P.M.W. Gill, B. Johnson, W. Chen, M.W. Wong, J.L. Andres, C. Gonzalez, M. Head-Gordon, E.S. Replogle and J.A. Pople, Gaussian, Inc., Pittsburgh PA, 1998.
- [17] J. E. Ridley and M. C. Zerner, *Theo. Chim. Acta* **32**, 111 (1973).
M. C. Zerner, *Semiempirical Molecular Orbital Methods in Reviews of Computational Chemistry*, edited by K. B. Lipkowitz and D. B. Boyd (VCH Publishing, New York, 1991), vol. 2, pp. 313-365.
- [18] CAChe 3.1, Oxford Molecular Ltd., 1997.

- [19] Yu. N. Romanovskii (unpublished).
- [20] See, e.g., G. D. Mahan, *Many-Particle Physics*, 2nd edition (Plenum Press, New York, 1990).
- [21] M. Rohlfing and S. G. Louie, *Phys. Rev. Lett.* **82**, 1959 (1999).
J.-W. van der Horst, P. A. Bobbert, P. H. L. de Jong, M. A. J. Michels, G. Brocks and P. J. Kelly, *Phys. Rev. B* **61**, 15817 (2000).
- [22] D. Guo, S. Mazumdar, S. N. Dixit, F. Kajzar, F. Jarka, Y. Kawabe and N. Peyghambarian, *Phys. Rev. B* **48**, 1433 (1993).
- [23] E. Jeckelmann and R. J. Bursill, (private communication).
- [24] M. Knupfer, J. Fink, E. Zojer, G. Leising, and D. Fichou, *Chem. Phys. Lett.* **318**, 585 (2000).

FIGURES

FIG. 1. The LPPP oligomers; the substituents used by various experimental groups are summarized in Table I. In this work, all substituents are replaced by hydrogen.

FIG. 2. Optimized geometric structure of the $n = 0.5$ oligomere of LPPP on MP2/6-31G* level of theory.

FIG. 3. Calculated absorption spectra as a function of the oligomer length.

FIG. 4. Calculated energetic position of the optical transitions depending on the system size, compare Table IV. The experimental values for the $S_1 \leftarrow S_0$ transition are taken from [5].

FIG. 5. Calculated fluorescence lifetimes as a function of the system size, compare Table IV.

FIG. 6. For plotting $P_{s,0}(i, j)$ along a quasi one-dimensional chain, only those carbon atoms are into account which are marked with bold lines.

FIG. 7. $P_{S_{1,0}}(i, j) \equiv P_{ij}$ for the S_1 state of the oligomer with two phenylene rings ($n = 0.5$). The state is determined by finite-size effects of the molecule, i.e., there is no bound electron-hole pair.

FIG. 8. $P_{S_{1,0}}(i, j) \equiv P_{ij}$ for the S_1 state of the oligomer with five phenylene rings ($n = 2$). A bound Frenkel exciton is discernible.

FIG. 9. Expectation value $\langle E \rangle_{S_{1,0}}$ and standard deviation $\sigma_{S_{1,0}}$ for the state S_1 in units of Å as a function of the oligomer length.

FIG. 10. Smoothed distribution function $\overline{P}_{S_{1,0}}(r) \equiv \overline{P}_{ij}$ as a function of the separation r for the state S_1 for various oligomer lengths.

FIG. 11. Probability distribution $P_{S_{1,0}}(i, j) \equiv P_{ij}$ along a quasi one-dimensional path for the oligomers with eleven ($n = 5$) phenylene rings for the state S_1 .

FIG. 12. Expectation value $\langle E \rangle_{S_{m,0}}$ and standard deviation $\sigma_{S_{m,0}}$ for the state S_m in units of Å as a function of the oligomer length.

FIG. 13. Smoothed distribution function $\overline{P}_{S_{m,0}}(r) \equiv \overline{P}_{ij}$ as a function of the separation r for the state S_m for various oligomer lengths.

FIG. 14. Probability distribution $P_{S_m,0}(i,j) \equiv P_{ij}$ along a quasi one-dimensional path for the oligomers with eleven ($n = 5$) phenylene rings for the state S_m .

FIG. 15. Expectation value $\langle E \rangle_{S_F,0}$ and standard deviation $\sigma_{S_F,0}$ for the state S_F in units of \AA as a function of the oligomer length.

FIG. 16. Smoothed distribution function $\overline{P}_{S_F,0}(r) \equiv \overline{P}_{ij}$ as a function of the separation r for the state S_F for various oligomer lengths.

FIG. 17. Probability distribution $P_{S_F,0}(i,j) \equiv P_{ij}$ along a quasi one-dimensional path for the oligomers with eleven ($n = 5$) phenylene rings for the state S_F .

FIG. 18. Expectation value $\langle E \rangle_{H \rightarrow L,0}$ and standard deviation $\sigma_{H \rightarrow L,0}$ for the state $|\Phi_{H \rightarrow L}\rangle$ in units of \AA as a function of the oligomer length.

FIG. 19. Smoothed distribution function $\overline{P}_{H \rightarrow L,0}(r) \equiv \overline{P}_{ij}$ as a function of the separation r for the state $|\Phi_{H \rightarrow L}\rangle$ for various oligomer lengths.

FIG. 20. Probability distribution $P_{H \rightarrow L,0}(i,j) \equiv P_{ij}$ along a quasi one-dimensional path for the oligomers with (a) two ($n = 0.5$) and (b) eleven ($n = 5$) phenylene rings for the state $|\Phi_{H \rightarrow L}\rangle$.

TABLES

TABLE I. Aliphatic substituents as defined in figure 1.

	[2], [6]	[4], [5]	this work
R ₁	n-Hexyl	n-Hexyl	H
R ₂	p(n-Decyl)-phenyl	p(t-Butyl)-phenyl	H
R ₃	Methyl	H	H
R' ₁	H if terminus, R ₁ otherwise		

TABLE II. Comparison between MP2, AM1, and PM3.

Method	E / a.u. ^a	ZPE/(kcal · mol ⁻¹) ^b	point group	$\sum \Delta r_{C-C} $ ^c
MP2/6-31G*	-499.8413498	117.80	<i>C</i> _{2v}	-
AM1	0.0862897	121.55	<i>C</i> _{2v}	0.000
PM3	0.0778001	117.65	<i>C</i> _{2v}	0.029

^a E = electronic energy (MP2), heat of formation (AM1, PM3)

^b ZPE= zero point energy

^c $\sum |\Delta r_{C-C}|$ = Sum of the differences of the C-C bond lengths with respect to the optimized structure at MP2 level

TABLE III. Ground state energies of the LPPP oligomers at AM1 level.

N ^a	E/a.u. ^b	ZPE/(kcal · mol ⁻¹) ^c	E + ZPE /a.u.	point group
2	0.0862897	121.55	0.279986	<i>C</i> _{2v}
3	0.1373472	178.64	0.422035	<i>C</i> _{2h}
4	0.1883913	235.71	0.564020	<i>C</i> _{2v}
5	0.2394355	292.76	0.705985	<i>C</i> _{2h}
7	0.3415265	406.85	0.989898	<i>C</i> _{2h}
9	0.4436183	520.95	1.273804	<i>C</i> _{2h}
11	0.5457102	635.03	1.557695	<i>C</i> _{2h}

^a N = number of phenylene rings

^b E = heat of formation

^c ZPE= zero point energy

TABLE IV. Calculated energetic position of the transitions from the ground state in cm^{-1} to the S_1 , S_m , and S_F state, depending on the system size, and fluorescence lifetimes depending on the system size. The experimental values for the $S_1 \leftarrow S_0$ transition are taken from [5].

$1/n^a$	Experiment [5]	S_1	S_m	S_F	$\tau/10^{-12}\text{s}^b$
0.500	-	34745.8	-	47703.1	1789
0.3	29500	31214.5	-	47629.4	1683
0.250	-	29289.2	-	47145.2	1115
0.200	25700	28055.1	3861.4	46995.0	920
0.143	23800	26841.0	34345.4	46851.2	693
0.1	-	26187.2	31613.2	46758.9	560
0.09	-	25795.0	30272.1	46686.4	470
0.083	22100	-	-	-	-

^a n = number of monomer units

^b τ = fluorescence lifetime following equation (1)

TABLE V. Values of the expectation value $\langle E \rangle_{s,0}$ and the standard orientation $\sigma_{s,0}$ for the optically detectable states, depending on the size of the oligomers.

state	values ^b	N ^a						
		2	3	4	5	7	9	11
$ \Phi_{H \rightarrow L}\rangle$	$\langle E \rangle_{H \rightarrow L,0}$	2.93	3.86	4.76	5.64	9.01	9.07	10.79
	$\sigma_{H \rightarrow L,0}$	1.80	2.49	3.16	3.82	5.77	6.38	7.65
S_1	$\langle E \rangle_{S_1,0}$	2.34	2.96	3.37	3.58	3.79	3.87	3.90
	$\sigma_{S_1,0}$	1.13	1.91	2.35	2.59	2.82	2.91	2.96
S_m	$\langle E \rangle_{S_m,0}$	-	-	-	3.06	3.05	3.20	3.52
	$\sigma_{S_m,0}$	-	-	-	2.18	2.19	2.21	2.59
S_F	$\langle E \rangle_{S_F,0}$	1.99	2.12	2.74	2.64	3.90	3.59	3.80
	$\sigma_{S_F,0}$	1.33	1.49	2.09	2.03	3.56	3.11	3.39

^a N = number of phenylene rings

^b $[\langle E \rangle] = [\sigma] = 1 \text{ \AA}$

FIG. 1. Jörg Rissler *Phys. Rev. B*

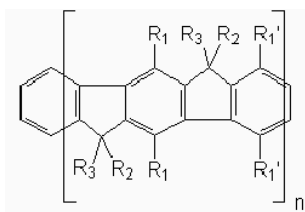


FIG. 2. Jörg Rissler *Phys. Rev. B*

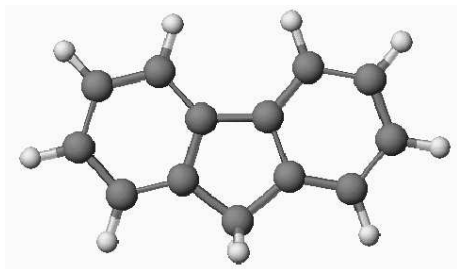


FIG. 3. Jörg Rissler *Phys. Rev. B*

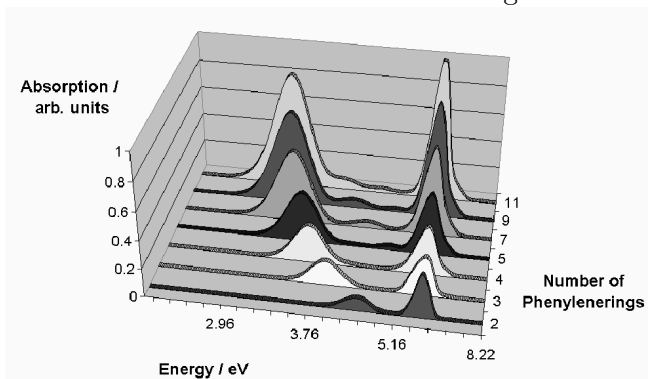


FIG. 4. Jörg Rissler *Phys. Rev. B*

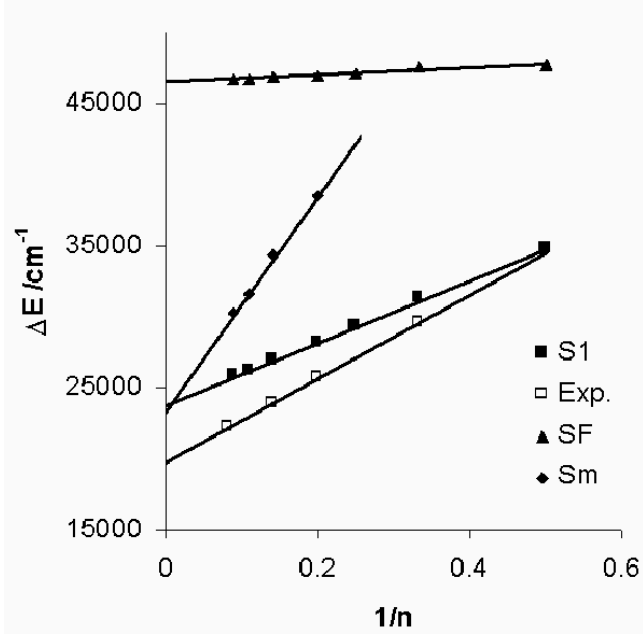


FIG. 5. Jörg Rissler *Phys. Rev. B*

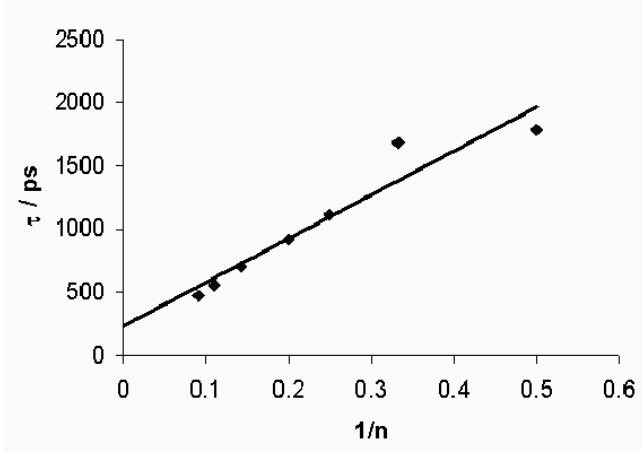


FIG. 6. Jörg Rissler *Phys. Rev. B*

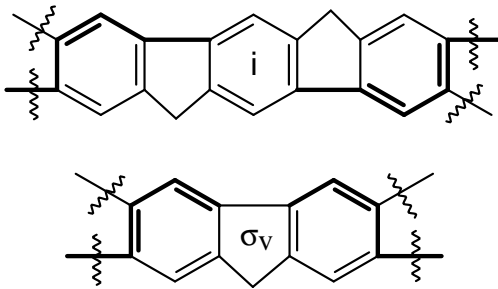


FIG. 7. Jörg Rissler *Phys. Rev. B*

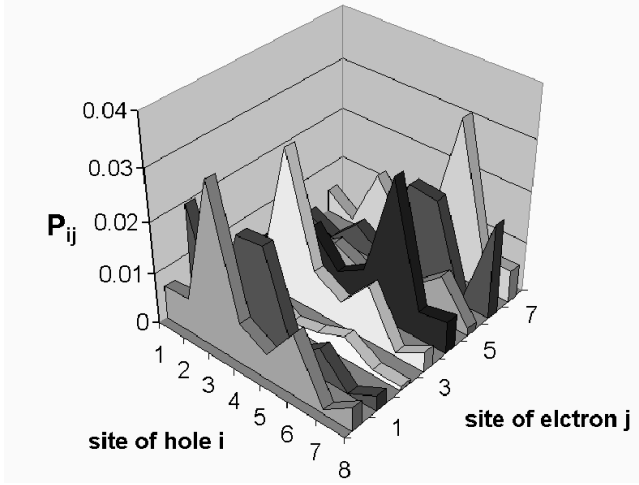


FIG. 8. Jörg Rissler *Phys. Rev. B*

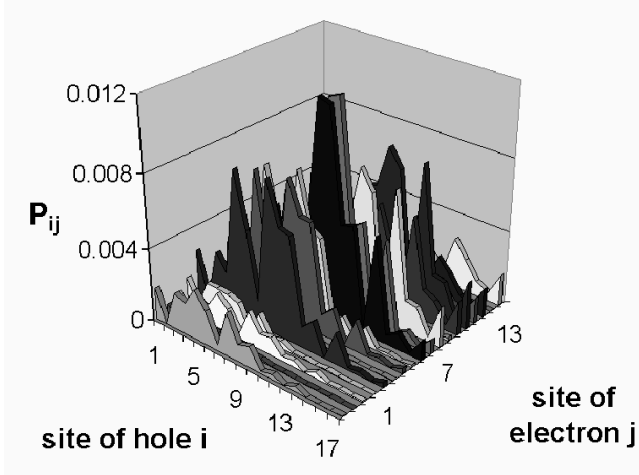


FIG. 9. Jörg Rissler *Phys. Rev. B*

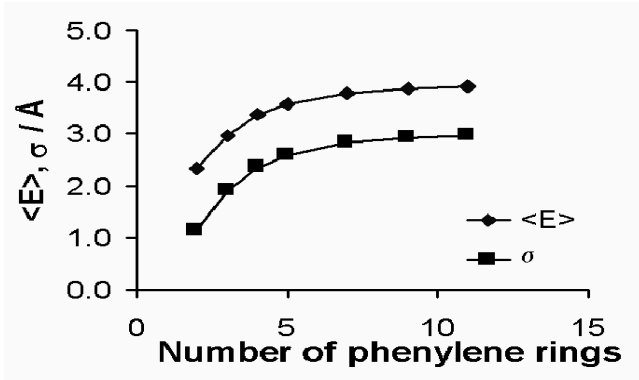


FIG. 10. Jörg Rissler *Phys. Rev. B*

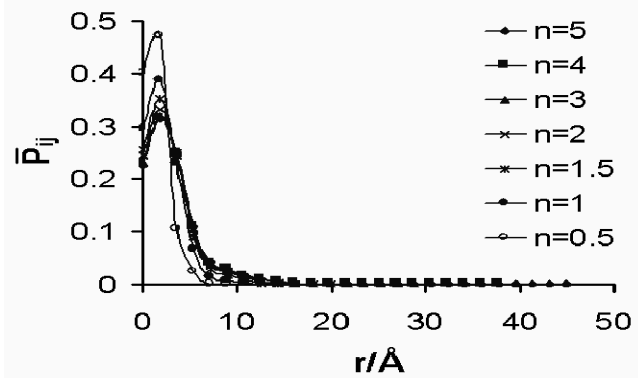


FIG. 11. Jörg Rissler *Phys. Rev. B*

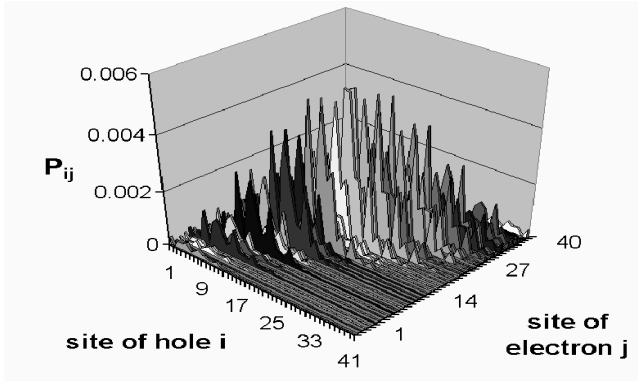


FIG. 12. Jörg Rissler *Phys. Rev. B*

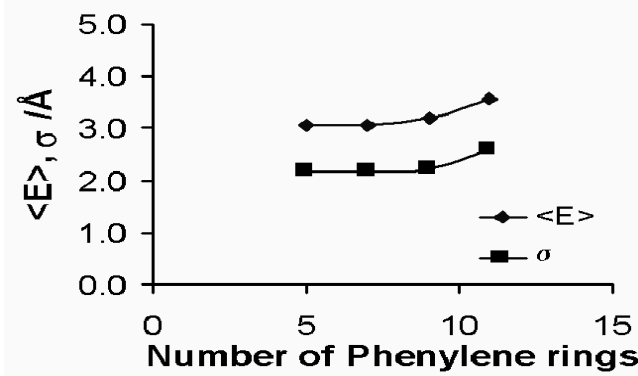


FIG. 13. Jörg Rissler *Phys. Rev. B*

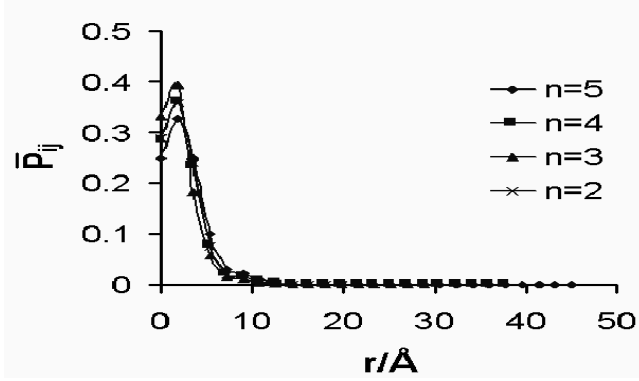


FIG. 14. Jörg Rissler *Phys. Rev. B*

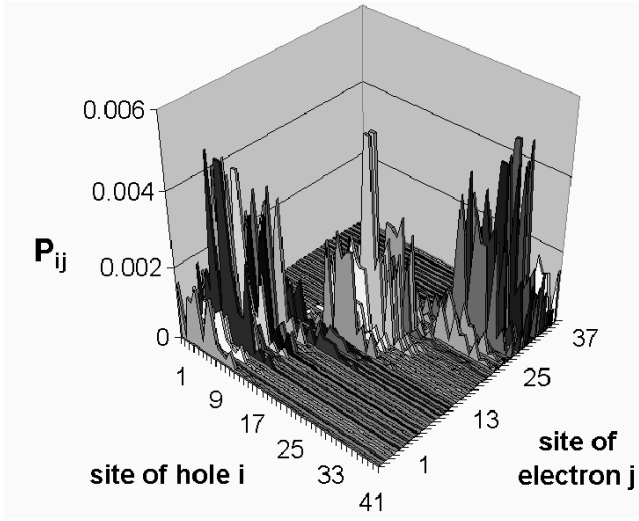


FIG. 15. Jörg Rissler *Phys. Rev. B*

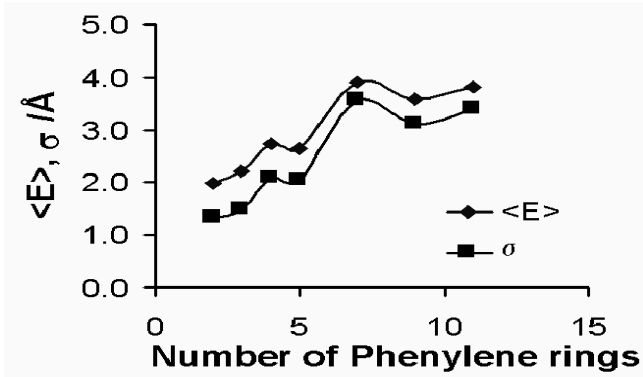


FIG. 16. Jörg Rissler *Phys. Rev. B*

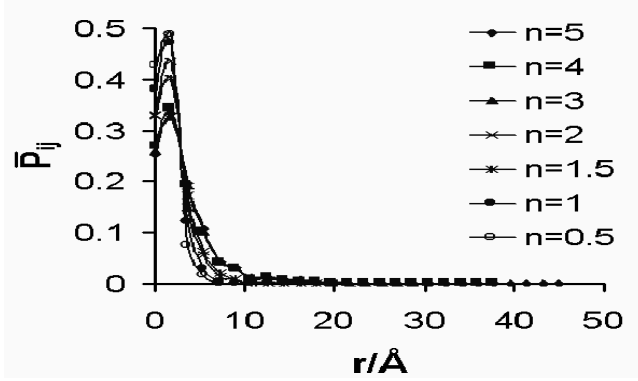


FIG. 17. Jörg Rissler *Phys. Rev. B*

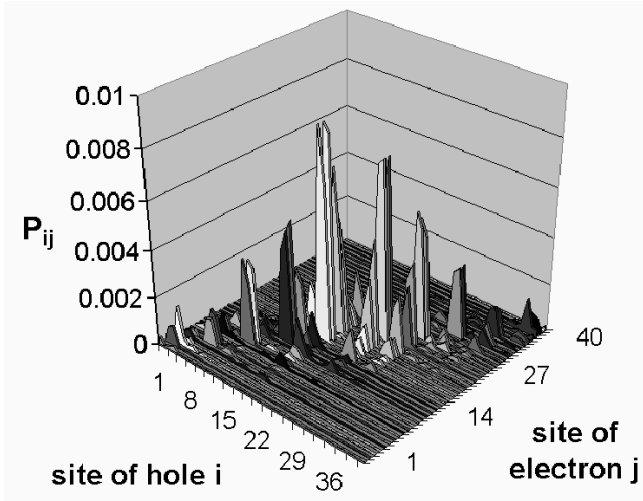


FIG. 18. Jörg Rissler *Phys. Rev. B*

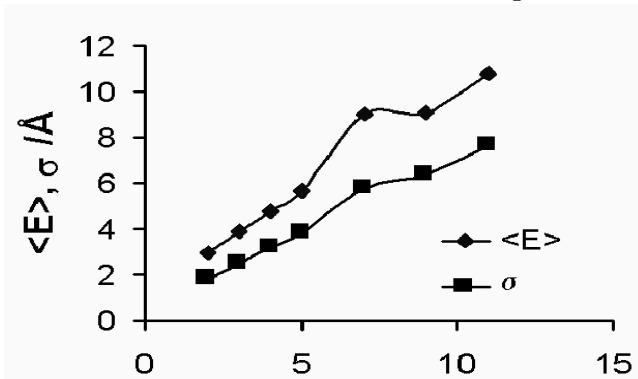


FIG. 19. Jörg Rissler *Phys. Rev. B*

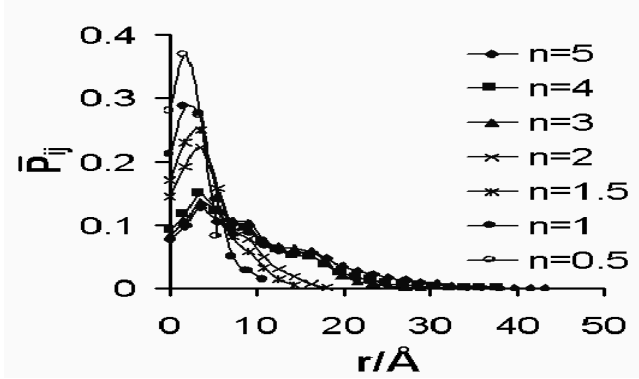


FIG. 20. Jörg Rissler *Phys. Rev. B*

